



OPEN Intelligent control algorithms for posture and height control of four-leg hydraulic supports

Yihui Pang^{1,2}✉ & Yaoyu Shi³

To address limitations of traditional inclinometers and height sensors in determining the posture and support height of hydraulic supports in coal mining, we propose a novel method predicated on travel measurements of the leg and tail beam cylinders. This method calculates the posture and height of hydraulic supports in mechanized mining. By conducting meticulous kinematic analysis of the hydraulic supports, a skeleton model of the main structural parameters of the hydraulic support was constructed. This approach transforms the traditional geometric relationship solutions of the main structure of the hydraulic supports into solutions based on the coordinate relationships of the main hinge points of the support, resulting in a mathematical expression for solving the support posture and height of the hydraulic supports. Meticulous algorithms for solving the support posture and height of hydraulic supports were developed based on the Newton–Raphson method, secant method, and Broyden’s method. The robustness, stability, calculation accuracy, and speed of these algorithms have been verified through analysis using the skeleton model and field measurement methods. The influence of initial coordinate parameters on the calculation results has been analyzed, and it was determined that the solution method based on the Newton–Raphson method has better robustness, stability, and calculation speed. The results of the research provide a theoretical foundation and technical support for precise, rapid control and intelligent management of hydraulic supports, effectively advancing the development of intelligent control systems for mining equipment.

Keywords Hydraulic support, Support posture, Tilt sensor, Skeletal model, Newton–Raphson method, Leg travel

The hydraulic support is the primary support device for controlling the stability of surrounding rock in mining areas. The support force and posture of the hydraulic support directly influence the stabilization efficacy of the surrounding rock mass. In recent years, with the rapid development of a new generation of intelligent sensing and automatic control technologies^{1–3}, there’s an increasing recognition of the importance of the support posture of the hydraulic support in controlling the surrounding rock. Consequently, the exploration of adaptive control techniques, predicated on the autonomous perception and exact computation of the support’s posture and elevation, has incrementally progressed. However, the efficient and accurate calculation of the support posture and height of the hydraulic support remains an unresolved challenge⁴. This is also a challenging issue in the development of intelligent equipment for coal mining.

To achieve automatic sensing and precise calculation of the support height and posture of the hydraulic support, existing technology primarily involves installing a tilt sensor on various components of the hydraulic support, such as the canopy, caving shield, connecting rod, base, and tail beam. Subsequently, a height-measuring sensor is positioned at the foremost extremity of the hydraulic support’s canopy. The data from these five sensors are integrated and analyzed to determine the support height and posture of the hydraulic support^{5,6}. Due to the current bottlenecks in intelligent sensing technology, the existing sensing techniques for support posture calculation exhibit several shortcomings:

- (1) Field measurements indicate that the stability of tilt sensors exhibit substandard stability. Even when the hydraulic support is stationary, there are still unwarranted fluctuations in the readings from the tilt sensors, which is not conducive to data collection.

¹Intelligent Mine Research Institute, Chinese Institute of Coal Science, Beijing 100013, China. ²Coal Mining Branch, China Coal Research Institute, Beijing 100013, China. ³School of Emergency Management and Safety Engineering, China University of Mining & Technology, Beijing 100083, China. ✉email: pangyihui0909@163.com

- (2) Current inclinometers poorly adapt to scenarios with large angles. Especially when the angle of inclination surpasses 60° , such as on the caving shield, four-link rods, and tail beam of the hydraulic support, the sensing accuracy drops significantly and the data fluctuation range increases noticeably.
- (3) Given that each hydraulic support requires the installation of five sensors, the location and quality of installation will significantly affect monitoring outcomes. This not only drives up the investment and maintenance costs but also intensifies the maintenance workload.
- (4) There exists a need to calibrate the time axis for all five sensors. Errors from each sensor can impact calculation results, leading to large accumulated errors. The data processing becomes complex and challenging, resulting in relatively low accuracy in the calculated outcomes.

To heighten the sensing accuracy and accelerate calculation speed of the support posture and height of hydraulic support, domestic and foreign scholars have conducted extensive and in-depth research. In the references^{7,8}, some scholars employed batch estimation methods and adaptive weighting methods to fuse sensory data from multiple tilt sensors. By optimizing the installation position of the tilt sensors, they derived a calculation method for the support posture and height of hydraulic support. However, the results are still affected by the sensing accuracy of multiple tilt sensors and data fluctuations. In the references^{9–11}, some scholars utilized machine vision techniques to monitor the support posture and height information of hydraulic support. They constructed an image recognition measurement model for the support posture of hydraulic support and employed Unity3D for simulating the support parameters of hydraulic support, exploring simulation control strategies based on the support posture. However, due to the confined spaces in coal mines, low illumination, and high dust operating environment, it's challenging for machine vision methods to achieve comprehensive sensing of the support posture of hydraulic support, ensuring both imaging quality and calculation accuracy. Kong et al.¹² proposed a sensor optimal placement method based on a discrete particle swarm optimization algorithm for optimizing the placement of sensors in hydraulic control systems. Chen et al.¹³ developed a multi-sensor fusion-based attitude monitoring system for advanced hydraulic supports in harsh underground environments, achieving high accuracy and stability with minimal root mean square errors in distance, roll angle, and yaw angle measurements. Zhang et al.¹⁴ proposed an adaptive sliding mode control method for the hydraulic support pushing mechanism in coal mine backfill operations, significantly improving system stability through decoupling analysis and simulation validation. Jiao et al.¹⁵ proposed a digital twin-driven intelligent decision-making method for the self-adjustment of the position and attitude of hydraulic support groups, enabling virtual decision-making and real-time control. In the references^{16–19}, some scholars employed various filtering and compensation algorithms to analyze the sensing data from tilt sensors, aiming to reduce the impact of data fluctuations on calculation results. They also endeavored to improve the sensing accuracy of tilt sensors in scenarios with large angles. However, the sensing accuracy of tilt sensors is not only influenced by the calculation method but is also constrained by physical components. The issue of irregular fluctuations in the sensing data from tilt sensors remains a challenge that needs to be effectively addressed.

This paper distinguishes itself by addressing the limitations of these existing methods. Based on the structural parameters and kinematic relationships of comprehensive mechanized hydraulic supports, it was determined that at least four tilt sensors and one height-measuring sensor are traditionally required for accurate calculations. To overcome the challenges of sensor limitations, this study introduces a novel algorithm that reduces the number of sensors from five to three by replacing tilt sensors with travel sensors. This algorithm focuses on the movement of front and rear legs and tail beam cylinders, enabling efficient and precise posture and height calculations in real-time. The proposed algorithm reduces data fluctuations and cumulative errors associated with tilt sensors. Lowers investment and maintenance costs. Improves computational efficiency and accuracy by simplifying data fusion. These innovations highlight the study's unique contributions, setting it apart from existing research. The findings provide theoretical foundations and technical solutions for the precise control of hydraulic supports, advancing intelligent management of mining equipment.

Hydraulic support skeleton model

The hydraulic support is mainly composed of a canopy, a caving shield, a tail beam, lemniscate link, a base, front legs, rear legs, and tail beam cylinders, as shown in Fig. 1. After establishing the model and structural parameters of the hydraulic support based on the requirements for controlling the surrounding rock in the mining area, the posture and height of the hydraulic support are primarily influenced by the travels of the front leg, rear leg, and tail beam cylinder^{20,21}. That is, there exists a one-to-one mapping relationship between the posture and height of the hydraulic support and the travels of the front leg, rear leg, and tail beam cylinder.

The support posture of the hydraulic support can be categorized into relative support posture and absolute support posture. The relative support posture refers to the relative positional relationship between various components of the hydraulic support, while the absolute support posture pertains to the positional relationship of the hydraulic support components relative to the ground's horizontal reference plane. By monitoring the relative positional relationship between the base of the hydraulic support and the ground's horizontal plane, the absolute support posture can be derived from the relative posture of the hydraulic support. Therefore, this paper primarily focuses on the algorithm for the relative support posture of the hydraulic support.

Using the upper surface of the hydraulic support's canopy as a reference plane, vertical projections of the hinge points of the front leg, rear leg, and canopy are made onto the canopy's upper surface. Furthermore, the hinge point where the canopy and caving shield intersect is also projected vertically onto the canopy's upper surface. Using the upper surface of the hydraulic support's caving shield as a reference plane, vertical projections are made for the hinge points of the four-link mechanism, tail beam, and tail beam cylinder onto the caving shield's upper surface. Furthermore, the hinge point where the canopy and caving shield intersect is also projected vertically onto the caving shield's upper surface. Using the bottom surface of the base as a reference,

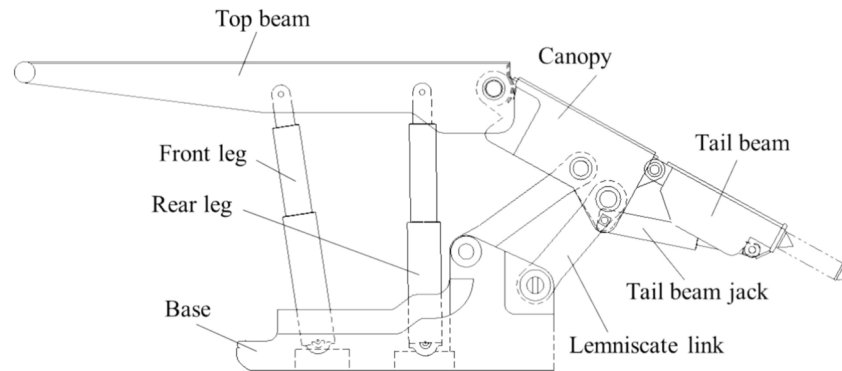


Fig. 1. Main structure of the comprehensive mechanized hydraulic support.

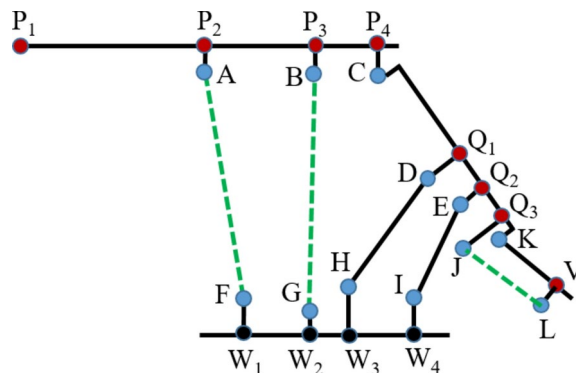


Fig. 2. Skeleton model of the comprehensive mechanized mining hydraulic support.

vertical projections are made of the hinge points of the front leg, rear leg, and the four-link mechanism onto the bottom surface of the base. These projections construct the skeletal model of the four-leg chock-shielded hydraulic support in comprehensive mechanized mining, as illustrated in Fig. 2.

To facilitate description, the hinge points of the hydraulic support's skeletal model are labeled with letters. Specifically: Point A: the hinge point between the front leg and the canopy. Point B: the hinge point between the rear leg and the canopy. Point C: the hinge point between the canopy and the caving shield. Point D: the hinge point between the front link rod and the caving shield. Point E: the hinge point between the rear link rod and the caving shield. Point F: the hinge point between the front leg and the base. Point G: the hinge point between the rear leg and the base. Point H: the hinge point between the front link rod and the base. Point I: the hinge point between the rear link rod and the base. Point J: the hinge point between the tail beam cylinder and the caving shield. Point K: the hinge point between the caving shield and the tail beam. Point L: the hinge point between the tail beam cylinder and the tail beam.

Considering the ZF10000/23/45D type of the four-leg chock-shielded hydraulic support, applied by Henan Energy Chemical Group Co., Ltd., as an example: once the model and structural parameters of the hydraulic support have been determined, there are only three variables for the hydraulic support. Moreover, the support height and support posture of the hydraulic support are solely controlled by these three variables, which are the travel of the front leg, the travel of the rear leg, and the travel of the tail beam cylinder. By surveying and mapping the main structural parameters of the ZF10000/23/45D hydraulic support in the field and constructing its skeletal model using the aforementioned method, a rectangular coordinate system is established for the sake of subsequent analysis and calculation. The projection of the base's bottom surface onto the coordinate plane serves as the x-axis, and the projection line of point P1 at the front end of the canopy onto the x-axis, when the hydraulic support is at its maximum support height (and the canopy is parallel to the base), serves as the y-axis. The parameters of the hydraulic support's skeletal model are illustrated in Fig. 3 and Table 1.

Support posture and height analysis method

Mathematical expression for the algorithm of support posture and height

To facilitate the calculation of the hydraulic support's posture and height, the following assumptions are made:

- (1) It is assumed that the hinge points between the various components of the hydraulic support are rigidly connected, the influence of the assembly clearance between the pin shaft and pin hole on the hydraulic support's posture is neglected.

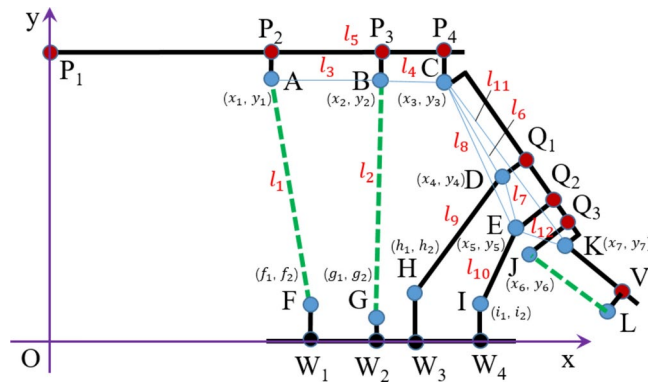


Fig. 3. Structural parameters and skeletal model of the ZF10000/23/45D hydraulic support.

Serial numbers	Identifier	Symbol	Parameter value/mm	Serial numbers	Identifier	Symbol	Parameter value/mm
1	AF	l_1	Variable	13	JC	l_{13}	2225.8
2	BG	l_2	Variable	14	JD	l_{14}	538
3	AB	l_3	1395.8	15	P_3B	l_{15}	238
4	BC	l_4	671.4	16	P_2A	l_{16}	287
5	AC	l_5	2065	17	Q_1D	l_{17}	557.7
6	CD	l_6	1700.8	18	Q_2E	l_{18}	640
7	DE	l_7	399.2	19	JL	l_{19}	Variable
8	CE	l_8	2100	20	JK	l_{20}	685.6
9	DH	l_9	1800	21	KL	l_{21}	977.1
10	EI	l_{10}	1700	22	P_1P_2	l_{22}	2545.5
11	KC	l_{11}	2370.6	23	$\angle VKL$	θ	13°
12	KE	l_{12}	584	24	$\angle AP_1P_2$	τ	6°

Table 1. Skeletal model parameters of the ZF10000/23/45D hydraulic support.

- (2) It is assumed that there is no significant deformation of the hydraulic support during the support process, the deformation of the hydraulic support material’s influence on the support posture is disregarded.
- (3) The support is treated as a plane mechanism.

Existing algorithms primarily employ tilt sensors to monitor the angles of the canopy, caving shield, or four-link mechanism, base, and tail beam. The posture of the hydraulic support is then determined based on the angular relationships between these components. The calculation process involves extensive trigonometric calculations, leading to significant cumulative errors²². Some researchers have attempted to construct a kinematic relationship model of the hydraulic support based on the geometric relationships of its structural components’ movements, aiming to determine the hydraulic support’s support posture. However, since the number of kinematic equations is less than the number of unknown parameters, obtaining an effective analytical solution proves challenging²³.

This study introduces an algorithm for calculating the posture and height of hydraulic supports based on a skeletal model and its geometric parameters. The algorithm utilizes a system of equations derived from the distance relationships among the coordinates of various hinge points in the model. By computing these coordinates, the hydraulic support’s posture and height are accurately determined. This method not only reduces the need for multiple sensors but also minimizes computational errors common in trigonometric solutions. For the ZF10000/23/45D hydraulic support model, the coordinate position relationship equations for each hinge point are established based on their distance relationships.

$$\left\{ \begin{array}{l} (x_1 - f_1)^2 + (y_1 - f_2)^2 = l_1^2 \\ (x_2 - g_1)^2 + (y_2 - g_2)^2 = l_2^2 \\ (x_1 - x_2)^2 + (y_1 - y_2)^2 = l_3^2 \\ (x_2 - x_3)^2 + (y_2 - y_3)^2 = l_4^2 \\ (x_1 - x_3)^2 + (y_1 - y_3)^2 = l_5^2 \\ (x_3 - x_4)^2 + (y_3 - y_4)^2 = l_6^2 \\ (x_4 - x_5)^2 + (y_4 - y_5)^2 = l_7^2 \\ (x_3 - x_5)^2 + (y_3 - y_5)^2 = l_8^2 \\ (x_4 - h_1)^2 + (y_4 - h_2)^2 = l_9^2 \\ (x_5 - i_1)^2 + (y_5 - i_2)^2 = l_{10}^2 \\ (x_7 - x_3)^2 + (y_7 - y_3)^2 = l_{11}^2 \\ (x_7 - x_5)^2 + (y_7 - y_5)^2 = l_{12}^2 \\ (x_6 - x_3)^2 + (y_6 - y_3)^2 = l_{13}^2 \\ (x_6 - x_4)^2 + (y_6 - y_4)^2 = l_{14}^2 \end{array} \right. \quad (1)$$

In the equation, $(x_1, y_1), (x_2, y_2), \dots, (x_7, y_7)$ are the coordinate values for points A, B, C, D, E, J, and K, respectively. The coordinate values vary with the travels of the front and rear legs. $(f_1, f_2), (g_1, g_2), (h_1, h_2), (i_1, i_2)$ are the fixed known coordinate values for points F, G, H, and I, respectively.

Based on the field monitoring results, by substituting the front leg travel value (l_1) and the rear leg travel value (l_2) into Eq. (1), the coordinates of points A, B, C, D, E, J, and K can be determined.

By independently analyzing the canopy skeletal model of the hydraulic support and considering the structural design requirements of the hydraulic support, there are potentially two scenarios regarding the vertical distance from the hinge points of the front leg, rear leg, and canopy to the upper surface of the canopy, as shown in Fig. 4.

(1) If $l_{16} \geq l_{15}$, the canopy state of the hydraulic support can be divided into the following three situations, as shown in Fig. 4(a).

Case 1: The vertical coordinate value of point A is not less than the vertical coordinate value of point B ($y_1 \geq y_2$). In this scenario, the canopy of the hydraulic support presents a significant “high angle” state. Based on the geometric relationship between the coordinates, the inclination angle α of the canopy relative to the base can be determined:

$$\alpha = \arctan \frac{y_1 - y_2}{x_2 - x_1} + \arcsin \frac{l_{16} - l_{15}}{l_3} \quad (2)$$

Case 2: The vertical coordinate value of point A is less than the vertical coordinate value of point B ($y_1 < y_2$), and $y_1 - y_2 \leq l_{16} - l_{15}$. In this scenario, the canopy of the hydraulic support presents a slight “high angle” state, or the canopy is parallel to the base. The inclination angle α of the canopy relative to the base is determined as:

$$\alpha = \arcsin \frac{l_{16} - l_{15}}{l_3} - \arctan \frac{y_2 - y_1}{x_2 - x_1} \quad (3)$$

Case 3: The vertical coordinate value of point A is less than the vertical coordinate value of point B ($y_1 < y_2$), and $y_1 - y_2 > l_{16} - l_{15}$. In this scenario, the canopy of the hydraulic support presents a “downtilt” state. The inclination angle α of the canopy relative to the base is determined as:

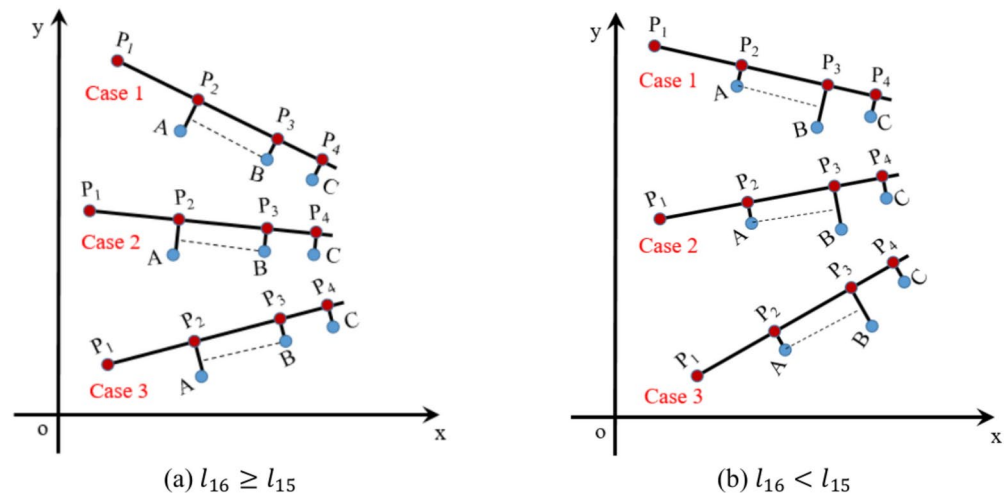


Fig. 4. Different support states of the hydraulic support’s canopy.

$$\alpha = 90^\circ - \arctan \frac{x_2 - x_1}{y_2 - y_1} - \arcsin \frac{l_{16} - l_{15}}{l_3} \tag{4}$$

(2) If $l_{16} < l_{15}$, the canopy state of the hydraulic support can be divided into the following three situations, as shown in Fig. 4(b).

Case 1: The vertical coordinate value of point A is greater than the vertical coordinate value of point B ($y_1 > y_2$), and $y_1 - y_2 \geq l_{15} - l_{16}$. In this scenario, the canopy of the hydraulic support presents a “high angle” state, or the canopy is parallel to the base. Based on the geometric relationship between the coordinates, the inclination angle α of the canopy relative to the base can be determined:

$$\alpha = 90^\circ - \arctan \frac{x_2 - x_1}{y_1 - y_2} - \arcsin \frac{l_{15} - l_{16}}{l_3} \tag{5}$$

Case 2: The vertical coordinate value of point A is greater than the vertical coordinate value of point B ($y_1 > y_2$), and $y_1 - y_2 < l_{15} - l_{16}$. In this scenario, the canopy of the hydraulic support presents a slight “downtilt” state. The inclination angle α of the canopy relative to the base is determined as:

$$\alpha = \arcsin \frac{l_{15} - l_{16}}{l_3} - \arctan \frac{y_1 - y_2}{x_2 - x_1} \tag{6}$$

Case 3: The vertical coordinate value of point A is less than or equal to the vertical coordinate value of point B ($y_1 \leq y_2$). In this scenario, the canopy of the hydraulic support presents a “downtilt” state. The inclination angle α of the canopy relative to the base is determined as:

$$\alpha = \arctan \frac{y_2 - y_1}{x_2 - x_1} + \arcsin \frac{l_{15} - l_{16}}{l_3} \tag{7}$$

By jointly analyzing the skeletal model of the caving shield, four-link mechanism, base, and tail beam of the hydraulic support, as shown in Fig. 5. According to the coordinates of points D and E, we can derive the expression for the angle β between the caving shield and the negative direction of the x-axis. Based on the coordinates of points D and H, we can determine the expression for the angle γ between the front linkage and the positive direction of the x-axis. By analyzing the coordinates of points E and I, we can calculate the angle δ between the rear linkage and the positive direction of the x-axis, as follows:

$$\begin{cases} \beta = 90^\circ - (\arctan \frac{x_5 - x_4}{y_4 - y_5} + \arcsin \frac{l_{17} - l_{18}}{l_7}) \\ \gamma = \arctan \frac{y_4 - h_2}{x_4 - h_1} \\ \delta = \arctan \frac{y_5 - i_2}{x_5 - i_1} \end{cases} \tag{8}$$

Given the coordinates of points J and K, and the travel of the tail beam cylinder l_{19} , which can be obtained from field measurements, the angle φ between the tail beam and the negative direction of the x-axis can be calculated.

$$\varphi = 90 - (\theta + \arccos \frac{l_{20}^2 + l_{21}^2 - l_{19}^2}{2 \cdot l_{20} \cdot l_{21}} - \arctan \frac{x_7 - x_6}{y_7 - y_6}) \tag{9}$$

Based on the coordinates of points P₁, P₂, and A, the protective height (H_c) of the front end of the hydraulic support canopy can be calculated. Specifically, this refers to the vertical projection distance from the front end of the canopy at point P₁ to the bottom surface of the base. The calculation primarily involves three scenarios:

Case 1: The canopy exhibits a “high angle” position or the canopy is parallel to the base ($\alpha \geq 0$):

$$H_c = l_{22} \times \sin\alpha + l_{16} \times \cos\alpha + y_1 \tag{10}$$

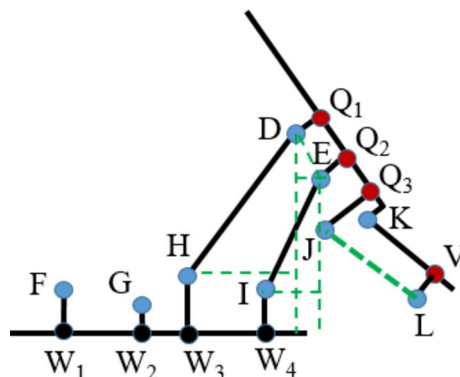


Fig. 5. Skeletal model of the caving shield, four-link mechanism, and base.

Case 2: The chock beam exhibits a “downtilt” status ($\alpha \geq 0$) and $|\alpha| \leq \tau$:

$$H_c = y_1 - l_{22} \times \sin(-\alpha) + l_{16} \times \cos\tau \quad (11)$$

Case 3: The chock beam exhibits a “downtilt” status ($\alpha \geq 0$) and $|\alpha| > \tau$:

$$H_c = y_1 - l_{16}/\sin(-\alpha) \times \sin(-\alpha - \tau) \quad (12)$$

From the analysis above, we can deduce that based on the stroke lengths of the front and rear legs, and the geometric relationship of the hydraulic support, the coordinates of each hinge point of the hydraulic support can be determined. Further, by utilizing the stroke length of the tail beam cylinder and the hydraulic support's geometric relationship, a mathematical representation of the hydraulic support's posture and height can be derived.

Solution based on the Newton–Raphson method

Based on the stroke of the hydraulic support's front leg, the stroke of the rear leg, the stroke of the tail beam cylinder, and the geometric relationship, we obtained the mathematical expression for the posture and height of the hydraulic support. However, it is challenging to solve the coordinates of each pivot point of the hydraulic support using a multivariate polynomial equation system. Consequently, we adopted the Newton–Raphson method^{24,25} for the computation. The aforementioned Eq. (1) is represented by the vector function $F(x)$ and expanded at the point $x^{(k)}$ using the Taylor series. To simplify the equation system's solution process, only the linear part of the Taylor series expansion is considered, as follows:

$$F(x) = \begin{cases} f_1(x_1, x_2, \dots, x_{12}) = 0 \\ \vdots \\ f_{12}(x_1, x_2, \dots, x_{12}) = 0 \end{cases} \quad (13)$$

$$F(x) \approx F(x^{(k)}) + F'(x^{(k)})(x - x^{(k)}) \quad (14)$$

where, $F'(x)$ is the Jacobian matrix of $F(x)$, as follows:

$$F'(x) = \begin{pmatrix} \frac{\partial f_1(x)}{\partial x_1} & \dots & \frac{\partial f_1(x)}{\partial x_{12}} \\ \vdots & \dots & \vdots \\ \frac{\partial f_{12}(x)}{\partial x_1} & \dots & \frac{\partial f_{12}(x)}{\partial x_{12}} \end{pmatrix} \quad (15)$$

Based on the structural parameters and the operational height range of the hydraulic support, the coordinate values of points A, B, C, D, E, J, and K can be determined as the constraint conditions for the equation set. It can be proven that the equation set converges within this interval, implying the existence of a unique analytical solution. The iterative solution process is as follows:

$$x^{(k+1)} = x^{(k)} - F'(x^{(k)})^{-1} F(x^{(k)}) \quad (16)$$

For convenience in obtaining the initial iteration parameters $x^{(0)}$, one can take the coordinates of each point obtained when the hydraulic support is at its highest support position in the coordinate system shown in Fig. 3 as the initial parameters $x^{(0)}$. Based on the actual support requirements of the field working face, the support posture error of the hydraulic support should be less than 2° , and the support height error should be less than 0.1 m. Therefore, the termination condition ε for iteration can be determined as:

$$\frac{\|x^{(k+1)} - x^{(k)}\|}{x^{(k)}} < \varepsilon \quad (17)$$

To facilitate the calculation of the support posture and height of the hydraulic support, an algorithm based on the Newton–Raphson method was developed using Python software. This algorithm was tested and verified on the ZF10000/23/45D hydraulic support to analyze the calculation precision and speed. The front leg travel of the hydraulic support was adjusted to 1837 mm, the rear hydraulic leg travel to 1811.7 mm, and the tail beam cylinder travel to 873.7 mm. The actual state of the hydraulic support's skeletal model is shown in Fig. 6. The above algorithm ran on a computer with a Win10 system, i7-7700 processor, and 32 GB RAM, and the calculation results are shown in Table 2.

After analyzing the computation results, it was observed that the deviation of the computed hydraulic support posture from the skeletal model's measured value was only 0.58° . The discrepancy between the computed support height and the measured value from the skeletal model was only 1.6 mm. The computation process took only 0.89 s. This implies that the hydraulic legosed computation algorithm is both accurate and efficient, meeting the precision requirements of field engineering applications.

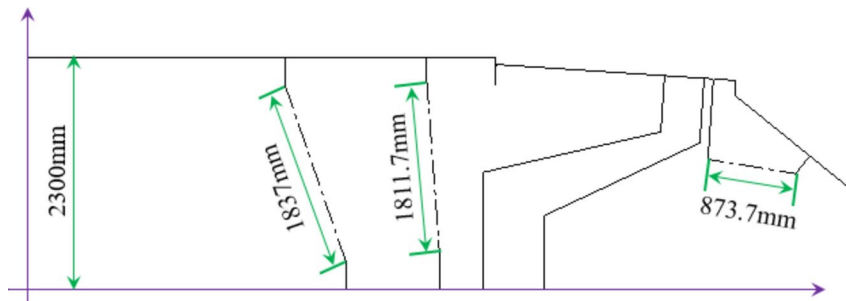


Fig. 6. Actual support posture of the hydraulic support.

Identifier	Coordinates	Initial parameters $x^{(0)}$	Actual value	Calculated result
A	(x_1, y_1)	(2545, 3913)	(2545.5, 2012.1)	(2572.3, 2013.7)
B	(x_2, y_2)	(3940, 3962)	(3940.4, 2061.9)	(3967.2, 2062.1)
C	(x_3, y_3)	(4610, 3920)	(4610.5, 2018.8)	(4637.3, 2019.3)
D	(x_4, y_4)	(5640, 2565)	(6248.1, 1559.4)	(6273.2, 1554.3)
E	(x_5, y_5)	(5881, 2248)	(6632.3, 1451.3)	(6657.2, 1445.1)
J	(x_6, y_6)	(5848, 2070)	(6713.3, 1289.3)	(6737.6, 1282.6)
K	(x_7, y_7)	(6441, 2414)	(6979.1, 1921.3)	(7005.5, 1914)
F	(f_1, f_2)	(3165, 275)	Known Fixed Values	
G	(g_1, g_2)	(4095, 255)	Known Fixed Values	
H	(h_1, h_2)	(4515, 1160)	Known Fixed Values	
I	(i_1, i_2)	(5115, 730)	Known Fixed Values	
α	-	-	0°	0.02°
β	-	-	4°	3.97°
γ	-	-	13°	12.36°
δ	-	-	25°	24.88°
φ	-	-	39°	39.58°
H_c	-	-	2300	2301.6
Computation Time T/s				0.89

Table 2. Results from the Newton–Raphson method.

Solution based on the Secant method

The Newton–Raphson method requires the computation of the Jacobian matrix $F'(x)$ for the system of equations. To reduce the need for differentiating the system of equations, the Jacobian matrix $F'(x)$ in the Taylor expansion can be replaced by finite differences^{26,27}. This leads to a modification of Eq. (14) as follows:

$$F(x) \approx F(x^{(k)}) + \frac{F(x^{(k)}) - F(x^{(k-1)})}{x^{(k)} - x^{(k-1)}}(x - x^{(k)}) \tag{18}$$

Consequently, the solution method for the posture of the hydraulic support based on the Secant method can be established as follows:

$$x^{(k+1)} = x^{(k)} - \left(\frac{F(x^{(k)}) - F(x^{(k-1)})}{x^{(k)} - x^{(k-1)}} \right)^{-1} F(x^{(k)}) \tag{19}$$

The Secant method based solution algorithm for the posture and height of the hydraulic support was developed using the Python software. The algorithm was run on the same computer, employing the following stroke values: 1837 mm for the front hydraulic leg, 1811.7 mm for the rear hydraulic leg, and 873.7 mm for the tail beam cylinder. The solution outcomes and computation speed of the Secant method are shown in Table 3.

After analyzing the computed results, it's clear that the outcomes from the Secant method closely match those from the Newton–Raphson method, meeting the accuracy needs for field engineering applications. However, the computational duration of approximately 13.57 s limits the solution's efficiency, posing challenges for real-time calculations.

Identifier	Coordinates	Initial parameters $x^{(0)}$	Actual value	Calculated result
A	(x_1, y_1)	(2545, 3913)	(2545.5, 2012.1)	(2572.3, 2013.7)
B	(x_2, y_2)	(3940, 3962)	(3940.4, 2061.9)	(3967.2, 2062.1)
C	(x_3, y_3)	(4610, 3920)	(4610.5, 2018.8)	(4637.3, 2019.3)
D	(x_4, y_4)	(5640, 2565)	(6248.1, 1559.4)	(6273.2, 1554.3)
E	(x_5, y_5)	(5881, 2248)	(6632.3, 1451.3)	(6657.2, 1445.1)
J	(x_6, y_6)	(5848, 2070)	(6713.3, 1289.3)	(6737.6, 1282.6)
K	(x_7, y_7)	(6441, 2414)	(6979.1, 1921.3)	(7005.5, 1914)
F	(f_1, f_2)	(3165, 275)	Known Fixed Values	
G	(g_1, g_2)	(4095, 255)	Known Fixed Values	
H	(h_1, h_2)	(4515, 1160)	Known Fixed Values	
I	(i_1, i_2)	(5115, 730)	Known Fixed Values	
α	–	–	0°	0.02°
β	–	–	4°	3.97°
γ	–	–	13°	12.36°
δ	–	–	25°	24.88°
φ	–	–	39°	39.58°
H_c	–	–	2300	2301.6
Computation Time T/s				13.57

Table 3. Results of the Secant method solution.

Solutions based on the Broyden method

To avoid the derivation of the Jacobian matrix $F'(x)$ in the Newton–Raphson method, a constant matrix A_k can be constructed to replace the Jacobian matrix $F'(x)$, as follows:

$$x^{(k)} = x^{(k-1)} - (A_k)^{-1} F(x^{(k-1)}) \quad (20)$$

Let $s^{(k)} = x^{(k)} - x^{(k-1)}$ and $y^{(k)} = F(x^{(k)}) - F(x^{(k-1)})$, then:

$$A_k s^{(k)} = y^{(k)} \quad (21)$$

Based on the Sherman–Morrison formula^{28,29}, the inverse of the matrix A_k can be obtained as follows:

$$A_k^{-1} = A_{k-1}^{-1} + \frac{(s^{(k)} - A_{k-1}^{-1} y^{(k)}) s^{(k)T} A_{k-1}^{-1}}{s^{(k)T} A_{k-1}^{-1} y^{(k)}} \quad (22)$$

The iterative solution process based on the above relationship is determined as follows:

$$x^{(k+1)} = x^{(k)} - A_k^{-1} F(x^{(k)}) \quad (23)$$

A software program was developed using Python to implement the Broyden method for solving the posture and height of the comprehensive mechanized mining hydraulic support system. The program was executed on the same computer with the same input values for the front leg stroke, rear leg stroke, and tail beam cylinder stroke (1837 mm, 1811.7 mm, and 873.7 mm, respectively). The results obtained using Broyden method and the computation speed are presented in Table 4.

After analyzing the calculation results, it was found that the solutions obtained using Broyden method are essentially the same as those using the Newton–Raphson method. They meet the precision requirements for field engineering calculations. However, the calculation process took about 4.83 s, making its efficiency lower than the Newton–Raphson method but slightly higher than the Secant method.

Results and discussion

Field measurement analysis

To validate the robustness and reliability of the described comprehensive methods for determining the posture and height of the hydraulic support, and to assess the effect of the gaps between pinholes and pin shafts on the calculation results, an field measurement analysis of the ZF10000/23/45D hydraulic support was carried out in the manufacturing workshop of Ningxia Tiandi Support Co., Ltd. The strokes of the front leg, rear leg, and tail beam cylinders of the hydraulic support were adjusted. Consequently, the hydraulic support was positioned such that the canopy was essentially parallel to the base, in a “high angle” position, and in a “downtilt” position, as depicted in Fig. 7.

External tension sensors measured the travels of the front leg, rear leg, and tail beam cylinder of the hydraulic support, facilitating the calculation of its posture and height. Fix both ends of the sensor to the fixed section

Identifier	Coordinates	Initial parameters $x^{(0)}$	Actual value	Calculated result
A	(x_1, y_1)	(2545, 3913)	(2545.5, 2012.1)	(2572.3, 2013.7)
B	(x_2, y_2)	(3940, 3962)	(3940.4, 2061.9)	(3967.2, 2062.1)
C	(x_3, y_3)	(4610, 3920)	(4610.5, 2018.8)	(4637.3, 2019.3)
D	(x_4, y_4)	(5640, 2565)	(6248.1, 1559.4)	(6273.2, 1554.3)
E	(x_5, y_5)	(5881, 2248)	(6632.3, 1451.3)	(6657.2, 1445.1)
J	(x_6, y_6)	(5848, 2070)	(6713.3, 1289.3)	(6737.6, 1282.6)
K	(x_7, y_7)	(6441, 2414)	(6979.1, 1921.3)	(7005.5, 1914)
F	(f_1, f_2)	(3165, 275)	Known Fixed Values	
G	(g_1, g_2)	(4095, 255)	Known Fixed Values	
H	(h_1, h_2)	(4515, 1160)	Known Fixed Values	
I	(i_1, i_2)	(5115, 730)	Known Fixed Values	
α	–	–	0°	0.02°
β	–	–	4°	3.97°
γ	–	–	13°	12.36°
δ	–	–	25°	24.88°
φ	–	–	39°	39.58°
H_c	–	–	2300	2301.6
Computation Time T/s				4.83

Table 4. Results of the Broyden method calculation.

and the movable section of the leg, respectively, to measure the elongation of the leg. Additionally, an angle measuring instrument assessed the angles of the canopy, protective beam, front linkage, rear linkage, and tail beam in relation to the base. For vertical distance measurements from the front end of the canopy to the base's bottom surface, a laser rangefinder was employed. A comparison between theoretical calculations and actual field measurements is presented in Fig. 8.

Through the analysis of the calculation results, it was found that all three algorithms demonstrate high precision in determining the support posture and height of the hydraulic support. Each of the three algorithms exhibited good robustness and stability. The measurements indicate that the assembly gap between the pin shaft and pinhole of the hydraulic support has little impact on the calculation results, and it meets the precision requisites for field engineering. Among the three algorithms, the Newton–Raphson method has the highest calculation speed, with an average computation time of less than 1 s, satisfying the field engineering requirements for calculation speed.

Analysis of the impact of initial parameters

Through the analysis of the solution principles of the three algorithms, it was found that the initial coordinate parameters $x^{(0)}$ in the solving process of Eq. (1) might affect the calculation precision and speed. Therefore, three sets of initial coordinate parameters were selected: For the first set ($x^{(0-1)}$), the initial coordinates were chosen randomly, but it should be ensured that Eq. (13) is differentiable. For the second set ($x^{(0-2)}$), the initial coordinates corresponded to the hydraulic support at a support height of 4.2 m. For the third set ($x^{(0-3)}$), the initial coordinates were from the hydraulic support at its lowest support height. The stroke values for the front and rear legs, as well as the tail beam cylinder, were still chosen based on the three sets of field measurements. The results of the calculations are shown in Table 5.

By analyzing the calculation results of different initial coordinate parameters, it was found that the selection of initial coordinate parameter values influences both the computational accuracy and velocity. For the first set ($x^{(0-1)}$), where initial coordinates were chosen randomly, the selected values were quite different from the final calculated coordinates. Furthermore, there was no correlation between various coordinate points, leading to a significant decrease in both precision and speed of the Newton–Raphson method. The Secant method and Broyden method both experienced calculation errors and memory overflow, failing to produce valid analytical solutions. For the second ($x^{(0-2)}$) and third ($x^{(0-3)}$) sets, where initial coordinates corresponded to the actual coordinates of the hydraulic support in its highest and lowest support states respectively, the results obtained from both initial coordinate sets were basically the same. The results from all three algorithms were consistent, though there was a noticeable difference in calculation speed. Since the gap between the third set ($x^{(0-3)}$) initial coordinates and the final target coordinate values was smaller, it achieved the fastest calculation speed.

Comparative analysis of calculation methods

The Newton–Raphson method, the Secant method, and the Broyden method were used to calculate the coordinate values of the hinge points of the main components of the integrated hydraulic support. Based on the mathematical expressions for the support posture and height of the hydraulic support, the angles between the canopy, protective beam, front linkage, rear linkage, tail beam, and base, as well as the support height from the front end of the canopy to the bottom surface of the base, were derived. A comparative analysis of the three algorithms indicated that the Newton–Raphson method exhibited the superior robustness and stability. Even



(a) Canopy is essentially parallel to the base ($l_1 = 2305\text{mm}, l_2 = 2335\text{mm}, l_{19} = 1009\text{mm}$)



(b) Canopy in a "high angle" position ($l_1 = 2550\text{mm}, l_2 = 2285\text{mm}, l_{19} = 956\text{mm}$)



(c) Canopy in a "downtilt" position ($l_1 = 2100\text{mm}, l_2 = 2298\text{mm}, l_{19} = 1001\text{mm}$)

Fig. 7. Field measurement of hydraulic support in different support positions.

when initial coordinates were chosen randomly, it still produced results in a relatively short time. When the initial coordinates were set to the actual values at the maximum or minimum support heights of hydraulic support, the results from all three algorithms were nearly indistinguishable, underscoring high precision in calculations. However, noticeable differences existed in the calculation speeds, as illustrated in Fig. 9.

The comparative analysis of the three algorithms clearly indicates that the Newton–Raphson method achieves the fastest calculation speed. Specifically, when initial coordinates correspond to actual values at the hydraulic support's extremal heights, the method completes calculations in less than 1 s. In contrast, the Secant method, while generally slower and less stable, can occasionally achieve faster calculation speeds. The Broyden method, on the other hand, operates more quickly than the Secant method but does not equal the Newton–Raphson method in speed. The analysis identifies two major factors affecting calculation speed: the number of iterations and the duration of each iteration. The random selection of initial coordinate values often requires numerous iterative calculations to approximate the solution coordinates to the target coordinates closely. Field measurements of the hydraulic support's three operational statuses, being closer to the minimum height, require fewer iterations. Consequently, setting initial coordinates at the minimum support height enhances iteration speed compared to using the maximum support height. Nevertheless, for practical field engineering applications, it is advisable to select initial coordinates within the range of heights most frequently utilized by the hydraulic support.

The comparative analysis underscores the superiority of the Newton–Raphson method over the other two methods in calculating the posture and height of hydraulic supports. It demonstrates enhanced robustness, stability, and a faster computation speed. Consequently, the Newton–Raphson method has been selected as the preferred calculation approach for determining the posture and height of hydraulic supports. To reduce the computational iterations, it is recommended to choose a support posture that falls within the actual mining height

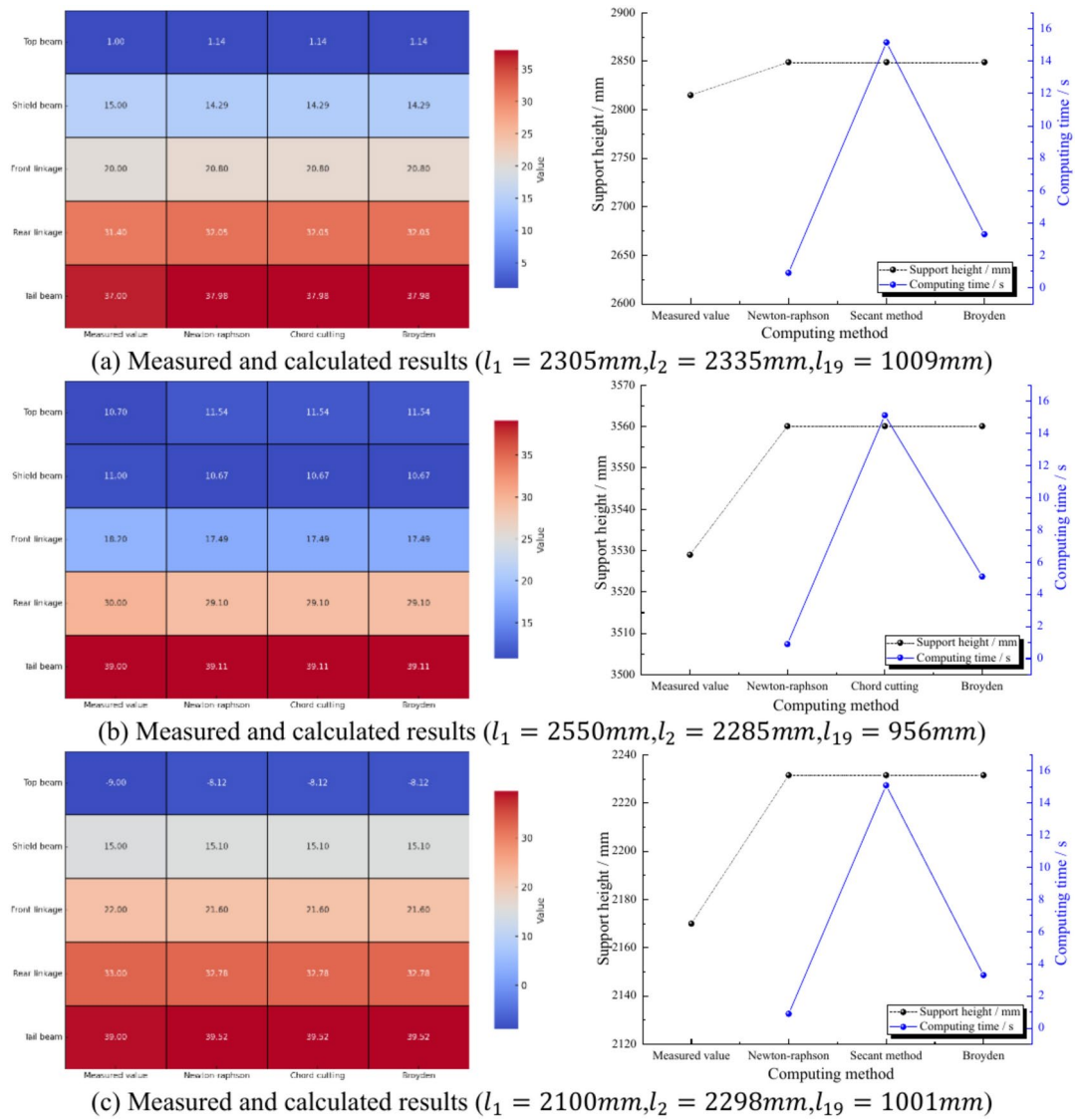


Fig. 8. Calculation results of different support states of the hydraulic support.

range of the working face. Utilizing the coordinate values from this specific posture as the initial parameters can significantly enhance calculation efficiency.

The algorithm introduced in this paper calculates the hydraulic support's posture and height based on the strokes of the hydraulic legs and tail beam cylinders. This approach not only reduces the number of required sensors but also guarantees stable monitoring values, as the strokes typically exhibit minimal fluctuation. Employing the Newton-Raphson method to determine the main structure's coordinate values effectively minimizes cumulative errors from trigonometric calculations. This provides a new approach for monitoring the support posture and height of hydraulic support.

While the proposed method offers significant advantages in speed and stability, future research will focus on optimizing the algorithm to enhance its adaptability to complex mining environments. For instance, in conditions with dust interference, low light, or extreme temperatures, sensor performance can be further validated and improved. Advanced data fusion techniques could be explored to integrate multiple sensor inputs, including machine vision or infrared sensing, for more comprehensive posture monitoring. Additionally, extending the algorithm to handle dynamic changes in support posture and real-time load adjustments will further strengthen its applicability in highly variable mining conditions. Future work will also explore the integration of digital twins to simulate and validate the algorithm in diverse operational scenarios, offering theoretical and practical advancements for intelligent mining systems.

Conclusions

- (1) The stroke values of the hydraulic legs and tail beam cylinders of the hydraulic support have a unique mapping relationship with the support posture. By extracting the skeletal structure parameter model of the

$x^{(0)}$	Stroke value/mm	Measured value	Newton–Raphson method	Secant method	Broyden method
$x^{(0-1)}$	Case 1: $l_1 = 2305$ $l_2 = 2335$ $l_{19} = 1009$	$\alpha:1^\circ, \beta:15^\circ,$ $\gamma:20^\circ, \delta:31.4^\circ,$ $\phi:37, H_c:2815$ mm	$\alpha:1.04^\circ, \beta:16.5^\circ,$ $\gamma:23.1^\circ, \delta:34.2^\circ,$ $\phi:26.1, H_c:2178$ mm T: 2.85 s	Error, memory overflow	Error, memory overflow
	Case 2: $l_1 = 2550$ $l_2 = 2285$ $l_{19} = 956$	$\alpha:10.7^\circ, \beta:11^\circ,$ $\gamma:18.2^\circ, \delta:30^\circ,$ $\phi:39, H_c:3529$ mm	$\alpha:11.4^\circ, \beta:13.1^\circ,$ $\gamma:19.7^\circ, \delta:31^\circ,$ $\phi:22.7, H_c:3552$ mm T: 2.85 s	Error, memory overflow	Error, memory overflow
	Case 3: $l_1 = 2100$ $l_2 = 2298$ $l_{19} = 1001$	$\alpha:-9^\circ, \beta:15^\circ,$ $\gamma:22^\circ, \delta:33^\circ,$ $\phi:39, H_c:2170$ mm	$\alpha:11.4^\circ, \beta:13.1^\circ,$ $\gamma:19.7^\circ, \delta:31^\circ,$ $\phi:22.7, H_c:3552$ mm T: 1.89 s	Error, memory overflow	Error, memory overflow
$x^{(0-2)}$	Case 1: $l_1 = 2305$ $l_2 = 2335$ $l_{19} = 1009$	$\alpha:1^\circ, \beta:15^\circ,$ $\gamma:20^\circ, \delta:31.4^\circ,$ $\phi:37, H_c:2815$ mm	$\alpha:1.14^\circ, \beta:14.3^\circ,$ $\gamma:20.8^\circ, \delta:32.1^\circ,$ $\phi:37.9, H_c:2849$ mm T: 0.91 s	$\alpha:1.14^\circ, \beta:14.3^\circ,$ $\gamma:20.8^\circ, \delta:32.1^\circ,$ $\phi:37.9, H_c:2849$ mm T: 15.16 s	$\alpha:1.14^\circ, \beta:14.3^\circ,$ $\gamma:20.8^\circ, \delta:32.1^\circ,$ $\phi:37.9, H_c:2849$ mm T: 3.1 s
	Case 2: $l_1 = 2550$ $l_2 = 2285$ $l_{19} = 956$	$\alpha:10.7^\circ, \beta:11^\circ,$ $\gamma:18.2^\circ, \delta:30^\circ,$ $\phi:39, H_c:3529$ mm	$\alpha:11.5^\circ, \beta:10.6^\circ,$ $\gamma:17.5^\circ, \delta:29.1^\circ,$ $\phi:39.1, H_c:3560.1$ mm T: 0.9 s	$\alpha:11.5^\circ, \beta:10.6^\circ,$ $\gamma:17.5^\circ, \delta:29.1^\circ,$ $\phi:39.1, H_c:3560.1$ mm T: 15.13 s	$\alpha:11.5^\circ, \beta:10.6^\circ,$ $\gamma:17.5^\circ, \delta:29.1^\circ,$ $\phi:39.1, H_c:3560.1$ mm T: 5.1 s
	Case 3: $l_1 = 2100$ $l_2 = 2298$ $l_{19} = 1001$	$\alpha:-9^\circ, \beta:15^\circ,$ $\gamma:22^\circ, \delta:33^\circ,$ $\phi:39, H_c:2170$ mm	$\alpha:-8.1^\circ, \beta:15.1^\circ,$ $\gamma:21.6^\circ, \delta:32.8^\circ,$ $\phi:39.5, H_c:2231.5$ mm T: 0.89 s	$\alpha:-8.1^\circ, \beta:15.1^\circ,$ $\gamma:21.6^\circ, \delta:32.8^\circ,$ $\phi:39.5, H_c:2231.5$ mm T: 15.1 s	$\alpha:-8.1^\circ, \beta:15.1^\circ,$ $\gamma:21.6^\circ, \delta:32.8^\circ,$ $\phi:39.5, H_c:2231.5$ mm T: 3.3 s
$x^{(0-3)}$	Case 1: $l_1 = 2305$ $l_2 = 2335$ $l_{19} = 1009$	$\alpha:1^\circ, \beta:15^\circ,$ $\gamma:20^\circ, \delta:31.4^\circ,$ $\phi:37, H_c:2815$ mm	$\alpha:1.14^\circ, \beta:14.3^\circ,$ $\gamma:20.8^\circ, \delta:32.1^\circ,$ $\phi:37.9, H_c:2849$ mm T: 0.67 s	$\alpha:1.14^\circ, \beta:14.3^\circ,$ $\gamma:20.8^\circ, \delta:32.1^\circ,$ $\phi:37.9, H_c:2849$ mm T: 14.9 s	$\alpha:1.14^\circ, \beta:14.3^\circ,$ $\gamma:20.8^\circ, \delta:32.1^\circ,$ $\phi:37.9, H_c:2849$ mm T: 1.62 s
	Case 2: $l_1 = 2550$ $l_2 = 2285$ $l_{19} = 956$	$\alpha:10.7^\circ, \beta:11^\circ,$ $\gamma:18.2^\circ, \delta:30^\circ,$ $\phi:39, H_c:3529$ mm	$\alpha:11.5^\circ, \beta:10.6^\circ,$ $\gamma:17.5^\circ, \delta:29.1^\circ,$ $\phi:39.1, H_c:3560.1$ mm T: 0.63 s	$\alpha:11.5^\circ, \beta:10.6^\circ,$ $\gamma:17.5^\circ, \delta:29.1^\circ,$ $\phi:39.1, H_c:3560.1$ mm T: 0.77 s	$\alpha:11.5^\circ, \beta:10.6^\circ,$ $\gamma:17.5^\circ, \delta:29.1^\circ,$ $\phi:39.1, H_c:3560.1$ mm T: 2.19 s
	Case 3: $l_1 = 2100$ $l_2 = 2298$ $l_{19} = 1001$	$\alpha:-9^\circ, \beta:15^\circ,$ $\gamma:22^\circ, \delta:33^\circ,$ $\phi:39, H_c:2170$ mm	$\alpha:-8.1^\circ, \beta:15.1^\circ,$ $\gamma:21.6^\circ, \delta:32.8^\circ,$ $\phi:39.5, H_c:2231.5$ mm T: 0.67 s	$\alpha:-8.1^\circ, \beta:15.1^\circ,$ $\gamma:21.6^\circ, \delta:32.8^\circ,$ $\phi:39.5, H_c:2231.5$ mm T: 14.67 s	$\alpha:-8.1^\circ, \beta:15.1^\circ,$ $\gamma:21.6^\circ, \delta:32.8^\circ,$ $\phi:39.5, H_c:2231.5$ mm T: 1.73 s

Table 5. Calculation results for different initial coordinate parameters.

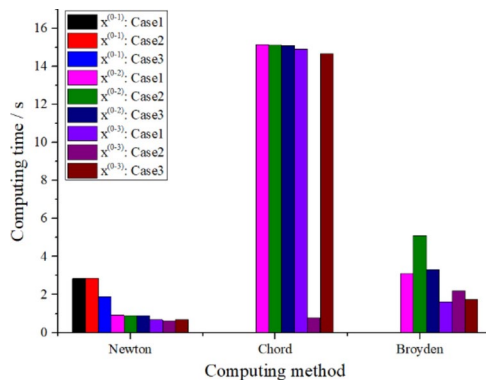


Fig. 9. Comparative analysis results of calculation speeds.

hydraulic support, a method for calculating the support posture and height of the hydraulic support based on the hydraulic leg stroke and tail beam cylinder stroke is proposed. This yields the mathematical expressions for the angles between the hydraulic support’s canopy, protective beam, connecting rods, tail beam, and base, as well as the method for calculating the support height at the front end of the canopy.

- (2) Algorithms based on the Newton–Raphson method, Secant method, and Broyden method for solving the support posture and height of the hydraulic support have been developed. When an appropriate initial coordinate parameter $x^{(0)}$ is selected, all three algorithms have high accuracy in solving the support posture and height of the hydraulic support. However, the Newton–Raphson method exhibits better robustness and reliability than the other two algorithms and has a faster solution speed.
- (3) The initial coordinate parameter $x^{(0)}$ can affect the iteration path and the number of iterations during the solution process, thereby influencing the accuracy and speed of the algorithm. The initial coordinate parameter $x^{(0)}$ should be selected as the real coordinate values of the support posture that the hydraulic sup-

port uses most frequently during the mining process. This can effectively reduce the number of iterations and improve the solution accuracy and speed.

- (4) The Newton–Raphson method-based algorithm has better accuracy, speed, robustness, and stability than the other two algorithms. It also has a stronger adaptability to the initial coordinate parameter $x^{(0)}$. The deviation between the calculated support posture and the actual value is less than 1° , and the deviation in support height is less than 50 mm. The single solution time does not exceed 1 s, which can meet the engineering requirements of coal mine sites.

Data availability

The authors confirm that the data supporting the findings of this study are available within the article.

Received: 9 November 2024; Accepted: 21 January 2025

Published online: 23 January 2025

References

- Ballard, Z., Brown, C., Madni, A. M. & Ozcan, A. Machine learning and computation-enabled intelligent sensor design. *Nat. Mach. Intell.* **3**, 556–565. <https://doi.org/10.1038/s42256-021-00360-9> (2021).
- Woodward, W. A., Gray, H. L. & Elliott, A. C. *Applied Time Series Analysis with R* (CRC Press, Boca Raton, 2016).
- Pech, M., Vrchota, J. & Bednár, J. Predictive maintenance and intelligent sensors in smart factory: Review. *Sensors* **21**, 1470. <https://doi.org/10.3390/s21041470> (2021).
- Cao, L., Sun, S., Zhang, Y., Guo, H. & Zhang, Z. The research on characteristics of hydraulic support advancing control system in coal mining face. *Wirel. Pers. Commun.* **102**, 2667–2680. <https://doi.org/10.1007/s11277-018-5294-4> (2018).
- Wang, G. & Pang, Y. Surrounding rock control theory and longwall mining technology innovation. *Int. J. Coal Sci. Technol.* **4**, 301–309. <https://doi.org/10.1007/s40789-017-0188-8> (2017).
- Ju, J. & Xu, J. Structural characteristics of key strata and strata behaviour of a fully mechanized longwall face with 7.0m Height chocks. *Int. J. Rock Mech. Min. Sci.* **58**, 46–54. <https://doi.org/10.1016/j.ijrmmms.2012.09.006> (2013).
- Xu, H. et al. A high precision fiber Bragg grating inclination sensor for slope monitoring. *J. Sens.* **2019**, e1354029. <https://doi.org/10.1155/2019/1354029> (2019).
- Shimizu, Y. et al. A liquid-surface-based three-axis inclination sensor for measurement of stage tilt motions. *Sensors* **18**, 398. <https://doi.org/10.3390/s18020398> (2018).
- Zeng, Q., Xu, W. & Gao, K. Measurement method and experiment of hydraulic support group attitude and straightness based on binocular vision. *IEEE Trans. Instrum. Meas.* **72**, 1–14. <https://doi.org/10.1109/TIM.2023.3267344> (2023).
- Zhang, Y., Zhang, H., Gao, K., Xu, W. & Zeng, Q. New method and experiment for detecting relative position and posture of the hydraulic support. *IEEE Access* **7**, 181842–181854. <https://doi.org/10.1109/ACCESS.2019.2958981> (2019).
- Penumuru, D. P., Muthuswamy, S. & Karumbu, P. Identification and classification of materials using machine vision and machine learning in the context of industry 4.0. *J. Intell. Manuf.* **31**, 1229–1241. <https://doi.org/10.1007/s10845-019-01508-6> (2020).
- Kong, X. et al. Optimal sensor placement methodology of hydraulic control system for fault diagnosis. *Mech. Syst. Signal Process.* **174**, 109069. <https://doi.org/10.1016/j.ymsp.2022.109069> (2022).
- Chen, H. et al. Research on attitude monitoring method of advanced hydraulic support based on multi-sensor fusion. *Measurement* **187**, 110341. <https://doi.org/10.1016/j.measurement.2021.110341> (2022).
- Zhang, Z., Liu, Y., Bo, L. & Wang, Y. Enhanced path tracking control of hydraulic support pushing mechanism via adaptive sliding mode technique in coal mine backfill operations. *Heliyon* **10**, e38437. <https://doi.org/10.1016/j.heliyon.2024.e38437> (2024).
- Jiao, X. et al. Intelligent decision method for the position and attitude self-adjustment of hydraulic support groups driven by a digital twin system. *Measurement* **202**, 111722. <https://doi.org/10.1016/j.measurement.2022.111722> (2022).
- Foxlin, E. Inertial head-tracker sensor fusion by a complementary separate-bias Kalman filter. In *Proceedings of the Proceedings of the IEEE 1996 Virtual Reality Annual International Symposium*, 185–194 (1996).
- Wang, G. et al. Research and practice of intelligent coal mine technology systems in China. *Int. J. Coal Sci. Technol.* **9**, 24. <https://doi.org/10.1007/s40789-022-00491-3> (2022).
- Huang, H. S. et al. Design on height measuring system of mine hydraulic powered support based on inclination sensor. *Coal Sci. Technol.* **46**(03), 124–129 (2018).
- Lu, T. K. et al. Design on posture dynamic monitoring and control system of hydraulic support. *Coal Sci. Technol.* **42**(S1), 169–170 (2014).
- Pang, Y., Wang, H., Lou, J. & Chai, H. Longwall face roof disaster prediction algorithm based on data model driving. *Int. J. Coal Sci. Technol.* **9**, 11. <https://doi.org/10.1007/s40789-022-00474-4> (2022).
- Xie, J., Wang, X., Yang, Z. & Hao, S. Virtual monitoring method for hydraulic supports based on digital twin theory. *Min. Technol.* **128**, 77–87. <https://doi.org/10.1080/25726668.2019.1569367> (2019).
- Zhang, K. et al. Height measurement method of hydraulic support based on multi-sensor data fusion. *Ind. Mine Autom.* **43**(09), 65–69 (2017).
- Lian, Z. S. et al. Networked intelligent sensing method for powered support. *J. China Coal Soc.* **45**(06), 2078–2089 (2020).
- Hartmann, S. A remark on the application of the Newton–Raphson method in non-linear finite element analysis. *Comput. Mech.* **36**, 100–116. <https://doi.org/10.1007/s00466-004-0630-9> (2005).
- Pho, K.-H. Improvements of the Newton–Raphson method. *J. Comput. Appl. Math.* **408**, 114106. <https://doi.org/10.1016/j.cam.2022.114106> (2022).
- Papakonstantinou, J. M. & Tapia, R. A. Origin and evolution of the secant method in one dimension. *Am. Math. Mon.* **120**, 500–517. <https://doi.org/10.4169/amer.math.monthly.120.06.500> (2013).
- Chen, Y. J. A iterative method with fast convergence speed: two-order parabola cut-chord method. *J. Foshan Univ. (Nat. Sci. Ed.)* **27**(5), 27–29 (2009).
- Maponi, P. The solution of linear systems by using the Sherman–Morrison formula. *Linear Algebra Appl.* **420**, 276–294. <https://doi.org/10.1016/j.laa.2006.07.007> (2007).
- Xie, J., Ge, F., Cui, T. & Wang, X. A virtual test and evaluation method for fully mechanized mining production system with different smart levels. *Int. J. Coal Sci. Technol.* **9**, 41. <https://doi.org/10.1007/s40789-022-00510-3> (2022).

Acknowledgements

This research was funded by the National Natural Science Foundation Project, Grant Number 52274154.

Author contributions

Writing—original draft preparation, conceptualization, funding acquisition, writing—review and editing, meth-

odology, project administration, Yi-hui Pang; formal analysis, software, writing—review and editing, Yao-yu Shi.

Declarations

Competing interests

The authors declare no competing interests.

Additional information

Correspondence and requests for materials should be addressed to Y.P.

Reprints and permissions information is available at www.nature.com/reprints.

Publisher's note Springer Nature remains neutral with regard to jurisdictional claims in published maps and institutional affiliations.

Open Access This article is licensed under a Creative Commons Attribution-NonCommercial-NoDerivatives 4.0 International License, which permits any non-commercial use, sharing, distribution and reproduction in any medium or format, as long as you give appropriate credit to the original author(s) and the source, provide a link to the Creative Commons licence, and indicate if you modified the licensed material. You do not have permission under this licence to share adapted material derived from this article or parts of it. The images or other third party material in this article are included in the article's Creative Commons licence, unless indicated otherwise in a credit line to the material. If material is not included in the article's Creative Commons licence and your intended use is not permitted by statutory regulation or exceeds the permitted use, you will need to obtain permission directly from the copyright holder. To view a copy of this licence, visit <http://creativecommons.org/licenses/by-nc-nd/4.0/>.

© The Author(s) 2025